Molecular Cancer Therapeutics

Relative Target Affinities of T-Cell–Dependent Bispecific Antibodies Determine Biodistribution in a Solid Tumor Mouse Model

Danielle Mandikian[1], Nene Takahashi[2], Amy A. Lo[1], Ji Li[1], Jeffrey Eastham-Anderson[1], Dionysos Slaga[1], Jason Ho[1], Maria Hristopoulos[1], Robyn Clark[1], Klara Totpal[1], Kedan Lin[3], Sean B. Joseph[4], Mark S. Dennis[5], Saileta Prabhu[1], Teemu T. Junttila[1], and C. Andrew Boswell[1]

Abstract

Anti-HER2/CD3, a T-cell–dependent bispecific antibody (TDB) construct, induces T-cell–mediated cell death in cancer cells expressing HER2 by cross-linking tumor HER2 with CD3 on cytotoxic T cells, thereby creating a functional cytolytic synapse. TDB design is a very challenging process that requires consideration of multiple parameters. Although therapeutic antibody design strategy is commonly driven by striving for the highest attainable antigen-binding affinity, little is known about how the affinity of each TDB arm can affect the targeting ability of the other arm and the consequent distribution and efficacy. To our knowledge, no distribution studies have been published using preclinical models wherein the T-cell–targeting arm of the TDB is actively bound to T cells. We used a combined approach involving radiochemistry, invasive biodistribution, and noninvasive single-photon emission tomographic (SPECT) imaging to measure TDB distribution and catabolism in transgenic mice with human CD3ε expression on T cells. Using CD3 affinity variants, we assessed the impact of CD3 affinity on short-term pharmacokinetics, tissue distribution, and cellular uptake. Our experimental approach determined the relative effects of (i) CD3 targeting to normal tissues, (ii) HER2 targeting to HER2-expressing tumors, and (iii) relative HER2/CD3 affinity, all as critical drivers for TDB distribution. We observed a strong correlation between CD3 affinity and distribution to T-cell–rich tissues, with higher CD3 affinity reducing systemic exposure and shifting TDB distribution away from tumor to T-cell–containing tissues. These observations have important implications for clinical translation of bispecific antibodies for cancer immunotherapy. *Mol Cancer Ther; 17(4); 776–85. ©2018 AACR.*

Introduction

Breast cancer is the leading cause of death for women from 20 to 59 years of age diagnosed with any cancer, with approximately 705 new cases diagnosed daily (1). About 15% to 20% of breast cancer overexpress the HER2 and are more likely to invade axillary lymph nodes than other subtypes (2). Approved antibody therapeutics that target HER2 include the monoclonal antibodies trastuzumab and pertuzumab and the antibody–drug conjugate ado-trastuzumab emtansine. However, low response rates and the emergence of resistance limit their efficacies (3).

A promising alternative therapeutic approach for treating multiple cancer types, including breast and other solid tumors, is T-cell–dependent bispecific (TDB) antibody therapy. TDBs are comprised of one arm targeting a cancer cell surface antigen and another arm targeting T-cell receptors (TCR) to engage the patient's immune system, most commonly through CD3. These bispecific molecules can bridge T cells to tumor cells through an artificial immunologic synapse (4), resulting in selective killing of target-expressing tumor cells which, in the case of CD3, occurs independently of the presence of MHC-I or costimulatory molecules (5). Targeting CD3 can lead to recruitment of both $CD8^+$ and $CD4^+$ T cells *in vivo* (6). Importantly, the mechanism of action requires that the TDB must bridge the T-cell together with the tumor cell; therefore, *in vivo* distribution of TDBs may affect this process based on relative affinities.

Bispecific antibodies in various formats have been explored as a means to recruit cytolytic T cells to treat various tumor types. Encouraging preclinical data have been obtained using CD3-engaging TDBs targeting B-cell lymphomas via both CD19 (7) and CD20 (8). Furthermore, impressive clinical data have emerged with molecules such as the B-cell tumor-targeting anti-CD19/CD3 bispecific T-cell engager (BiTE) blinatumomab (9). A similar TDB strategy has been applied to solid tumors for the treatment of $HER2^+$ breast cancers, including those resistant to approved HER2 therapeutics, at low picomolar concentrations in preclinical species, independent of HER2 signaling (10).

[1]Genentech, Inc., South San Francisco, California. [2]Northwestern University, Chicago, Illinois. [3]Department of Clinical Pharmacology, NGM Biopharmaceuticals Inc., South San Francisco, California. [4]Department of Pharmacology, Calibr, La Jolla, California. [5]Denali Therapeutics Inc., South San Francisco, California.

Note: Supplementary data for this article are available at Molecular Cancer Therapeutics Online (http://mct.aacrjournals.org/).

Corresponding Authors: C. Andrew Boswell, Genentech, Inc., 1 DNA Way, MS 463A, South San Francisco, CA 94080. Phone: 650-467-4603; Fax: 650-742-5234; E-mail: boswell.andy@gene.com; and Teemu T. Junttila, junttila.teemu@gene.com

doi: 10.1158/1535-7163.MCT-17-0657

Table 1. T-cell–dependent bispecific antibody monovalent affinities

Target	K_D[a] (nmol/L)
HER2	0.5
$CD3_{\varepsilon}L$	50
$CD3_{\varepsilon}H$	0.5
$CD3_{\varepsilon}VH$	0.05

[a]Monovalent K_D was determined using Biacore and reported as nmol/L values.

One issue that has not been fully explored is how affinity of each TDB binding arm affects *in vivo* distribution. With two distinct targeting arms, relative binding affinity could have a major impact on the overall TDB tissue distribution. Herein, we investigated how CD3 affinity alone affects the TDB's *in vivo* distribution and short-term systemic pharmacokinetics. We subsequently introduced the HER2-targeting arm to explore how competition between the two targets is affected by increasing CD3 affinity.

Materials and Methods

Generation of full-length CD3-bispecific antibodies

TDBs were generated using knobs-into-holes strategy (11) and purified as previously described (10). Three anti-human CD3ε molecules were used with different CD3ε affinities (CD3εL, "low," $K_D = 50$ nmol/L; CD3εH, "high," $K_D = 0.5$ nmol/L, and CD3εVH, "very high," $K_D = 0.05$ nmol/L). Affinities were measured by Biacore with human CD3εγ immobilized on chip and full-length bispecific antibody flown through, as previously described (12). To evaluate the effect of CD3 affinity in the absence of tumor target binding, we employed CD3 affinity variants in conjunction with target arms recognizing viral glycoprotein D (gD). To investigate the effect of T-cell affinity on the *in vivo* properties of an anti-HER2/CD3 TDB, we used a trastuzumab-based anti-HER2 arm (K_D 0.5 nmol/L; refs. 10, 13) paired with either low- or high-affinity CD3 arms (50 or 0.5 nmol/L), summarized in Table 1.

Radiochemistry

Iodine-125 [^{125}I] was obtained as sodium iodide in 0.1 N sodium hydroxide from Perkin Elmer. Note that 1 mCi of ^{125}I (~3 μL) was used to label randomly through tyrosine residues at a specific activity of approximately 10 μCi/μg with ^{125}I using the indirect Iodogen method (Pierce). Radiosynthesis of ^{111}In-labeled antibodies (~8 μCi/μg) was achieved through incubation of $^{111}InCl_3$ and 1,4,7,10-tetraazacyclododecane-1,4,7,10-tetraacetic acid (DOTA)–conjugated (randomly through lysines) mAb in 0.3 mol/L ammonium acetate pH 7 at 37°C for 1 hour. Purification of all radioimmunoconjugates was achieved using NAP5 columns equilibrated in PBS and confirmed by size-exclusion chromatography. To prevent thyroid sequestration of ^{125}I, 100 μL of 30 mg/mL of sodium iodide was intraperitoneally administered 1 and 24 hours prior to dosing.

Tissue distribution studies

The human CD3 epsilon transgenic (huCD3ε-TG) mice express both mouse and human CD3 on T cells (14). Incorporation of human CD3 to the TCR does not disturb normal T-cell development (14), and huCD3ε-TG T cells can kill human HER2-expressing target cells (10). The huCD3ε subunit can both structurally and functionally substitute for murine CD3ε in the transgenic mouse. In addition, the chimeric T-cell receptor in this model supports normal T-cell development and selection of repertoires *in vivo* and can mediate activity of the huCD3ε-specific HER2/CD3 bispecific antibody (14).

All animal experiments were conducted in accordance with an Institutional Animal Care and Use Committee. Biodistribution studies were performed in huCD3ε-TG mice bearing two different xenografts on each leg flank. CT26 cell lines were transfected to overexpress HER2. Xenografts of CT26 parental cells were inoculated on the left flank, whereas CT26-HER2 cells were inoculated on the right flank as previously described, reaching 200 mm^3 prior to TDB dosing (10).

Female huCD3ε-TG mice (20–30 g) were randomly assigned to groups ($n = 5$) and administered an intravenous bolus consisting of a mixture of ^{125}I- and ^{111}In-labeled TDB tracers (5 μCi of each) plus the respective unmodified antibody for a total dose of either 0.5 mg/kg (tracer groups) or 50.5 mg/kg (competition groups). Competition groups contained 50 mg/kg dose of nonradiolabeled bivalent antibody that could compete with a single arm of the TDB. Blood samples were collected from each animal at 1, 24, and 72 hours to derive plasma and whole-blood antibody concentrations. At 72 hours, tissue samples were promptly collected by terminal organ harvest and counted for radioactivity using a 1480 WIZARD Gamma Counter in the energy windows for ^{111}In (245 keV; decay $t_{1/2} = 2.8$ days) and ^{125}I (35 keV; decay $t_{1/2} = 59.4$ days) with automatic background and decay correction.

Cell lines

CT-26 cells were purchased from the ATCC. All other cell lines were obtained from Genentech's cell line core facility gCell. Short tandem repeat (STR) profiles were determined for each line using the Promega PowerPlex 16 System. This was performed once and compared with external STR profiles of cell lines (when available) to determine cell line ancestry. Sixteen different loci were detected (15 STR loci and Amelogenin for gender identification) including D3S1358, TH01, D21S11, D18S51, Penta E, D5S818, D13S317, D7S820, D16S539, CSF1PO, Penta D, AMEL, vWA, D8S1179, and TPOX. Cell lines were also determined to be mycoplasma free prior to use.

SPECT-CT

In vivo distribution was obtained by single-photon emission computed tomography/X ray computed tomography (SPECT-CT) imaging of huCD3ε-TG mice bearing CT26 and CT26-HER2 tumors with ^{111}In-labeled TDBs as previously described (15). Mice received an average dose of 405 μCi (range, 383–416 μCi) of ^{111}In-labeled antibodies for SPECT-CT or 5 μCi for invasive biodistribution analysis, at a dose of 5 mg/kg. Immediately after CT acquisition, SPECT was performed on the photopeaks of ^{111}In using a 5-pinhole collimator with 5.5 cm radius of rotation. Tissues were collected for gamma counting as in the nonimaging study arm. SPECT images were visualized using Amira software (TGS).

Image analysis

Data were analyzed and graphed using GraphPad Prism (version 7.00 for Windows). All values are expressed as mean ± SEM, and P values were assessed by unpaired, two-tailed, Student t test, unless otherwise indicated. $P < 0.05$ was considered statistically significant.

Results

Cellular binding of TDBs

Binding of gD/CD3 and HER2/CD3 to HER2-expressing SKBR3 cells was determined by flow cytometry. As expected, gD/CD3 TDBs did not bind to SKBR3 cells, whereas HER2/CD3$_\varepsilon$L and HER2/CD3$_\varepsilon$H showed similar binding profiles (Supplementary Fig. S1A). Similarly, CD3-expressing Jurkat cell lines were incubated with either gD/CD3 or HER2/CD3 TDBs with increasing CD3 affinity. As expected, Jurkat cell–binding profiles increased with CD3 affinity; however, the replacement of gD with the HER2 arm had no effect on CD3 binding (Supplementary Fig. S1B). Taken together, these data confirm expected cellular binding for the TDBs.

Characterization of dual tumor model

Several parameters of tumors may affect tumor distribution of CD3 bispecific antibodies including expression level of the tumor target, tumor vascularization, and level of T-cell infiltration in tumors. Significant differences between CT26 and CT26-HER2 tumors in above parameters would complicate interpretation of tumor distribution results and were therefore characterized in detail.

By Western blot and flow cytometry (Supplementary Fig. S2A and S2B) of the cell lines, CT26-HER2 cells express high levels of HER2. HER2 expression in CT26-HER2 cells was slightly lower than HER2-amplified SKBR3 and KPL4 cells, but substantially higher than MCF7. Further HER2 analysis was done from tumors excised from mice. Strong HER2 staining was detected in CD45$^-$ cells by flow cytometry (Supplementary Fig. S2C). Tumor sections were also stained using HER2 IHC (Supplementary Fig. S3A–S3D) and scored using ASCO-CAP, 2013 HER2 IHC guidelines for breast cancer. All CT26-HER2 tumors demonstrated heterogeneous, but strong positive (3+), HER2 staining that was most prominent at tumor nodule peripheries (Supplementary Fig. S3C and S3D). No HER2 expression was detected in parallel analysis of CT26 cells and tumors (Supplementary Figs. S2C, S3A and S3B).

Differential vascularization may affect tumor distribution of antibodies. Tumor vascularization in CT26 and CT26-HER2 tumors was assessed using MECA-32 (anti-PLVAP) IHC (Supplementary Fig. S4). MECA-32 staining was similar in both CT26-HER2– and CT26-derived xenografts (Supplementary Fig. S3I–S3L). Quantification of MECA-32–positive area (Supplementary Fig. S3M) and vessel perimeter (Supplementary Fig. S3N) showed no significant differences across HER2$^+$ and HER2$^-$ tumors, indicating equivalent vascularization.

Tumors were also analyzed for T-cell infiltration. Similar levels of T-cell infiltration were detected in CT26 tumors and CT26-HER2 tumors by flow cytometry (Supplementary Fig. S4A and S4B). In addition, tumor sections were stained using CD3ε IHC (Supplementary Fig. S3E–S3H). As expected, CD3ε staining intensities in tumor-derived T cells were identical between the models (Supplementary Fig. S3E–S3H). Both tumor models demonstrated similar levels of dispersed intratumoral CD3ε$^+$ cells. Peripheral regions of CT26-HER2 tumors demonstrated consistently more pronounced T-cell infiltration compared with CT26 tumors. Taken together, these data confirm that CT26-HER2 tumors express high levels of HER2 and indicate comparable vascular properties and baseline T-cell infiltration relative to the parental CT26 model.

Experimental system for TDB distribution studies

To quantitatively determine how CD3 affinity independently affects TDB distribution in the absence of a HER2-targeting arm, we performed biodistribution and limited pharmacokinetic (PK) studies using ^{111}In- and ^{125}I-labeled gD/CD3 TDBs. The dual-tracer approach can differentiate between intact and internalized/degraded TDB based on differences in biodistribution patterns of the attached radiotracers (15, 16). When iodinated antibodies (Fig. 1A) become internalized and degraded in lysosomes, the free-radioactive iodide and/or iodotyrosine rapidly diffuses from the cell and is cleared from systemic circulation. Consequently, the ^{125}I signal represents only intact antibody. In contrast, the same internalization and lysosomal degradation of ^{111}In-labeled antibodies (Fig. 1B) yields an ^{111}In-DOTA-amino acid adduct that is cell impermeable and accumulates over time. Therefore, subtracting ^{125}I signal from ^{111}In signal can be used to calculate the internalized/degraded (catabolized) antibody.

CD3 affinity does not affect anti-gD/CD3 TDB distribution to tumors

The effect of CD3 affinity on TDB distribution in the absence of HER2 binding was analyzed utilizing anti-gD/CD3 TDBs. HuCD3ε-TG mice bearing both CT26 parental and CT26-HER2 tumors (Fig. 1C) received a therapeutically relevant dose (0.5 mg/kg) of gD/CD3 TDBs. Table 1 lists the human affinities of each binding arm of the TDB. The effect of CD3 affinity on tissue distribution at 3 days and short-term systemic PK were measured (Fig. 2A). Due to limited sampling and study duration, PK parameters were not estimated, but short-term plasma exposures were calculated as AUC_{0-3d}. The plasma PK profile of the low (50 nmol/L) CD3 binder (gD/CD3εL) exhibited a comparable exposure to the bivalent anti-gD control antibody with mean AUC_{0-3d} values of 2,789 and 2,629 %ID/mL*day, respectively (Fig. 2B). Increasing CD3 affinity to 0.5 nmol/L (gD/CD3εH) and 0.05 nmol/L (gD/CD3εVH) caused a significant decrease in short-term systemic exposure with reduced mean AUC_{0-3d} values of 1,975 and 1,909 %ID/mL*day, respectively (Fig. 2B, $P < 0.001$ for both compared with gD control). Because plasma samples would not contain circulating T-cell–bound TDB, we also analyzed whole blood and cell pellet samples and observed no evidence of TDB sequestration or accumulation in circulating cells (Supplementary Fig. S5A and S5B).

All gD/CD3 TDBs distributed similarly to both tumors, comparable with a bivalent gD control antibody, ranging from 3.3 to 5.2 %ID/g with no significant differences across affinity variants or tumors (Fig. 2C). As expected, expression of HER2 by tumor cells had no effect on the distribution of anti-gD/CD3 TDBs. Distribution of intact (^{125}I-labeled) gD/CD3 TDBs in HER2-expressing tumors was 3.8 to 5.2 %ID/g and in HER2 nonexpressing tumors was 3.3 to 4.9 %ID/g (Fig. 2C). Catabolism was monitored by subtracting the ^{125}I %ID/g (intact) from ^{111}In %ID/g (intact and degraded). Similar to the intact antibody distribution, CD3 affinity did not affect catabolism in either tumor except for gD/CD3εVH. Coadministration of 100-fold excess of nonradiolabeled antibodies (Fig. 2C and D, "+ CD3 Block") did not induce competition for either intact or catabolized antibodies for most variants (Fig. 2C and D), suggesting that CD3 binding does not drive tumor distribution. The exception was slightly increased catabolism observed for gD/CD3εVH, potentially reflecting increased uptake by tumor-infiltrating T cells (Fig. 2D; ref. 10). The catabolism levels

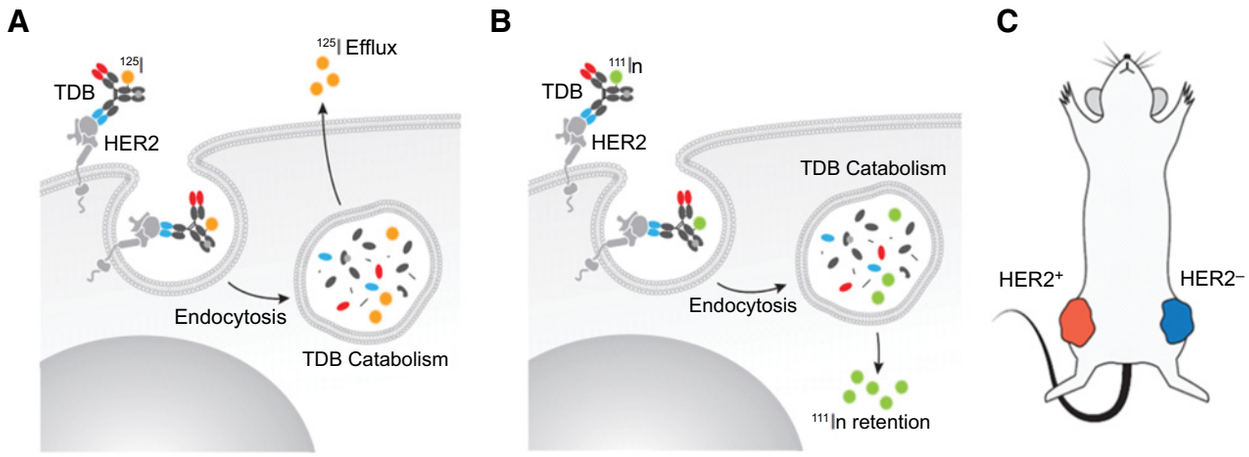

Figure 1.

Cellular metabolic pathways of radiolabeled antibodies and mouse model used in the tissue distribution studies. **A** and **B,** Schematic diagram of cellular metabolic pathways of radiolabeled antibodies. Upon target binding, the antibody–receptor complex is internalized and directed to lysosomes for degradation. The resulting radioadducts have cellular fates dependent on the radionuclide used for labeling. **A,** Molecular fates of ^{125}I-labeled antibodies. Catabolites of ^{125}I-labeled TDBs are free to diffuse across the cellular membrane, likely followed by entry to systemic circulation and renal clearance. **B,** Molecular fates of ^{111}In-DOTA–labeled antibodies. In contrast, the charged, polar catabolite of ^{111}In-DOTA-labeled TDBs, ^{111}In-DOTA-lysine, is unable to diffuse across the membrane and accumulates intracellularly over time. **C,** Schematic diagram of mouse model. Anti-human CD3 antibodies do not crossreact with murine CD3. To study the effect of huCD3 and HER2 affinities on pharmacokinetics and drug distribution, huCD3ε-TG mice were implanted with CT26- and huHER2-transfected-CT26 tumors on opposite flanks of the mice.

(~2 %ID/g) indicate that none of the gD/CD3 variants exhibited robust tumor cell internalization.

High CD3 affinity drives anti-gD/CD3 TDB distribution to secondary lymphatic organs

In addition to measuring tumor distribution of TDBs, we also determined how CD3 affinity, in the absence of tumor target arm binding, affects distribution to T-cell–containing tissues. Distribution to the spleen and lymph nodes was strongly correlated with CD3 affinity (Fig. 2E and F). The distribution profile of gD/CD3εL was similar to bivalent anti-gD control with %ID/g values under 2.5, indicating that 50 nmol/L affinity to CD3 on T cells is not sufficient to drive distribution to lymphatic organs. In striking contrast, gD/CD3 TDBs with subnanomolar (0.5 nmol/L) and picomolar (0.05 nmol/L) affinity exhibited significantly increased distribution to T-cell–containing tissues (Fig. 2E, $P < 0.05$ for all 3 variants in spleen and $P < 0.01$ for the gD/CD3εVH and gD/CD3εH in lymph nodes). Intact splenic distribution for gD/CD3εVH and gD/CD3εH was 3.8 and 2.6 %ID/g, respectively, whereas intact lymphatic distribution was 30 and 10.5 %ID/g. There was also significant catabolism of the CD3εH TDBs (5.3 %ID/g in spleen and 27.9 %ID/g in lymph nodes) and CD3εVH (7.1 %ID/g in spleen and 64.7 %ID/g in lymph nodes), suggesting robust internalization of high CD3 affinity TDBs in selected lymphoid organs (Fig 2F, $P < 0.001$ in spleen and $P < 0.01$ in lymph nodes). This finding, although seemingly contrasting with our data in tumor wherein little to no TDB catabolism occurred, may merely reflect a much higher enrichment of T cells in spleen and lymph nodes relative to tumor. Minimal catabolism of gD/CD3εL was observed (Fig. 2F). Competition assays using a coadministered 100-fold excess of nonradiolabeled gD/CD3 antibodies showed strongly reduced distribution and catabolism in T-cell–containing tissues, indicating that these processes were CD3 driven (Fig. 2E and F, $P < 0.05$). In summary, in the absence of HER2 binding, CD3 affinity does not affect tumor distribution. However, high affinity to T cells is correlated with increased distribution to T-cell–containing tissues and reduced plasma exposures.

High CD3 affinity disturbs HER2-dependent tumor distribution of anti-HER2/CD3 TDB

After characterizing the effects of isolated CD3 affinity on biodistribution, we studied how CD3 affinity affects distribution when paired with the tumor (HER2) targeting arm. Each radiolabeled anti-HER2/CD3 TDB variant was administered in a single IV bolus (0.5 mg/kg) to the double-tumor–bearing huCD3ε-TG mice, with limited plasma PK samples collected throughout the study followed by tissue distribution assessment at 3 days after injection (Fig. 3A). The short-term exposure of high CD3 affinity molecule (HER2/CD3εH, mean $AUC_{0-3d} = 2102$ %ID/mL*day) was lower compared with the low CD3 affinity antibody (HER2/CD3εL, mean $AUC_{0-3d} = 2438$ %ID/mL*day) over the course of 3 days (Fig 3B). The inverse correlation of systemic exposure with CD3 affinity was similar but less pronounced to that observed with gD/CD3 TDBs (13.8% vs. 24.9% reduction in AUC_{0-3d}, Figs. 2B and 3B). This key finding suggests that, when paired with HER2 targeting, CD3 affinity is not the sole driver of tissue distribution (i.e., TDBs leaving systemic circulation). We also analyzed whole blood and cell pellet samples and observed no evidence of TDB sequestration or accumulation in circulating cells (Supplementary Fig. S5C and S5D).

Distribution of HER2/CD3εL (7.2 %ID/g) to the HER2-expressing tumor was significantly higher compared with the HER2/CD3εH (4.8 %ID/g, $P < 0.05$; Fig. 3C). Blocking the HER2 arm with 100-fold excess of nonradiolabeled antibody significantly reduced distribution (2.3 %ID/g) and catabolism (2.6 %ID/g) of HER2/CD3εL to HER2$^+$ tumors (Fig. 3C and D; $P < 0.001$). This effect was weaker and not significant for the HER2/CD3εH

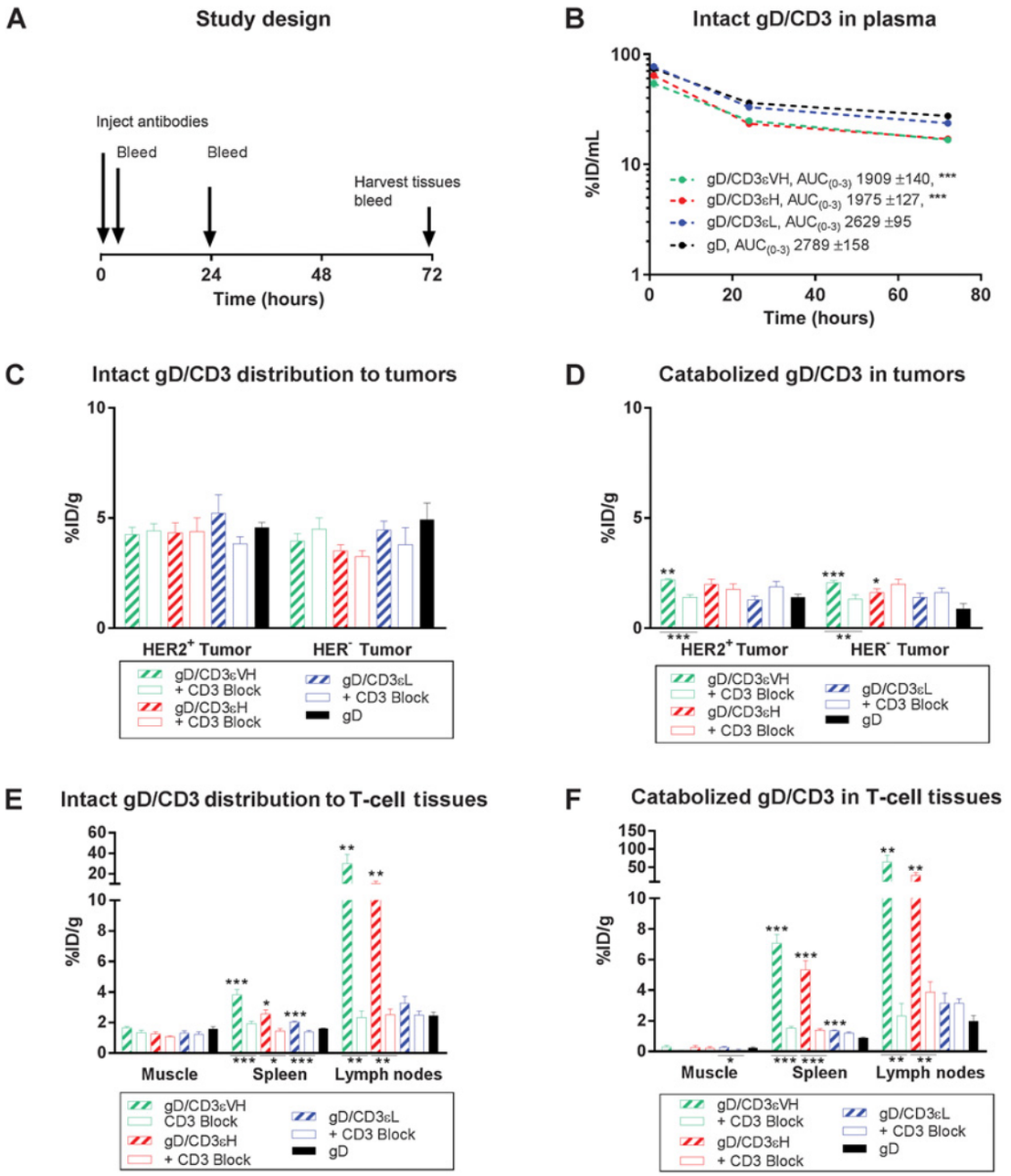

Figure 2.

CD3 affinity drives anti-gD/CD3 TDB distribution to T-cell–containing tissues, but not to tumor. **A,** Study design. The huCD3ε-TG mice bearing CT26 and huHER2-CT26 tumors on opposite flanks were injected with a single IV bolus of ^{125}I- and ^{111}In-labeled anti-gD/CD3 TDBs (0.5 mg/kg) with low (CD3εL), high (CD3εH), or very high (CD3εVH) affinity to human CD3. Sparse blood sampling was done at 1, 24, and 72 hours. At 72 hours, mice were sacrificed for tissue distribution. Values are reported as a percentage of injected radioactive dose normalized to gram of dry blotted tissue (%ID/g) to convey changes in enrichment. In the groups denoted as "Block," the radiolabeled 0.5 mg/kg anti-gD/CD3 TDB was coadministered with 50 mg/kg nonradiolabeled bivalent anti-CD3 antibody. **B,** Pharmacokinetics. Plasma levels of ^{125}I-radiolabeled antibody are represented as %ID/mL. AUC and AUC ± SEM values were calculated using GraphPad Prism with ***, $P < 0.001$ when compared with anti-gD. **C–F,** Tissue distribution. Tissue concentrations of intact anti-gD/CD3 antibodies expressed as ^{125}I (ID/g) in (**C**) tumor and (**E**) T-cell–containing tissues. Catabolized antibody values in tumors were determined by subtracting the ^{125}I (%ID/g) from the ^{111}In (%ID/g), and plotted as catabolism (%ID/g) in (**D**) tumors and (**F**) T-cell–containing tissues. All graphs are mean ± SEM for each group with $n = 5$. P values were obtained by the Student t test, and significance was determined by comparing each gD/CD3 TDB distribution to either anti-gD (a control IgG) or the corresponding CD3 block. Comparisons with anti-gD are indicated as significant with asterisks over the bars within each tissue. The CD3 block comparisons for each TDB are indicated under the bars, with lines confirming the direct comparison checked for significance in each tissue. In addition, to determine the impact of HER2 expression on CD3 distribution in tumors (**C–D**), CD3εL, CD3εH, and CD3εVH were compared with the counter group across HER2$^{+/-}$ tumors; however, results were not significant. All significant P values were reported as *, $P < 0.05$; **, $P \leq 0.01$; and ***, and $P \leq 0.001$.

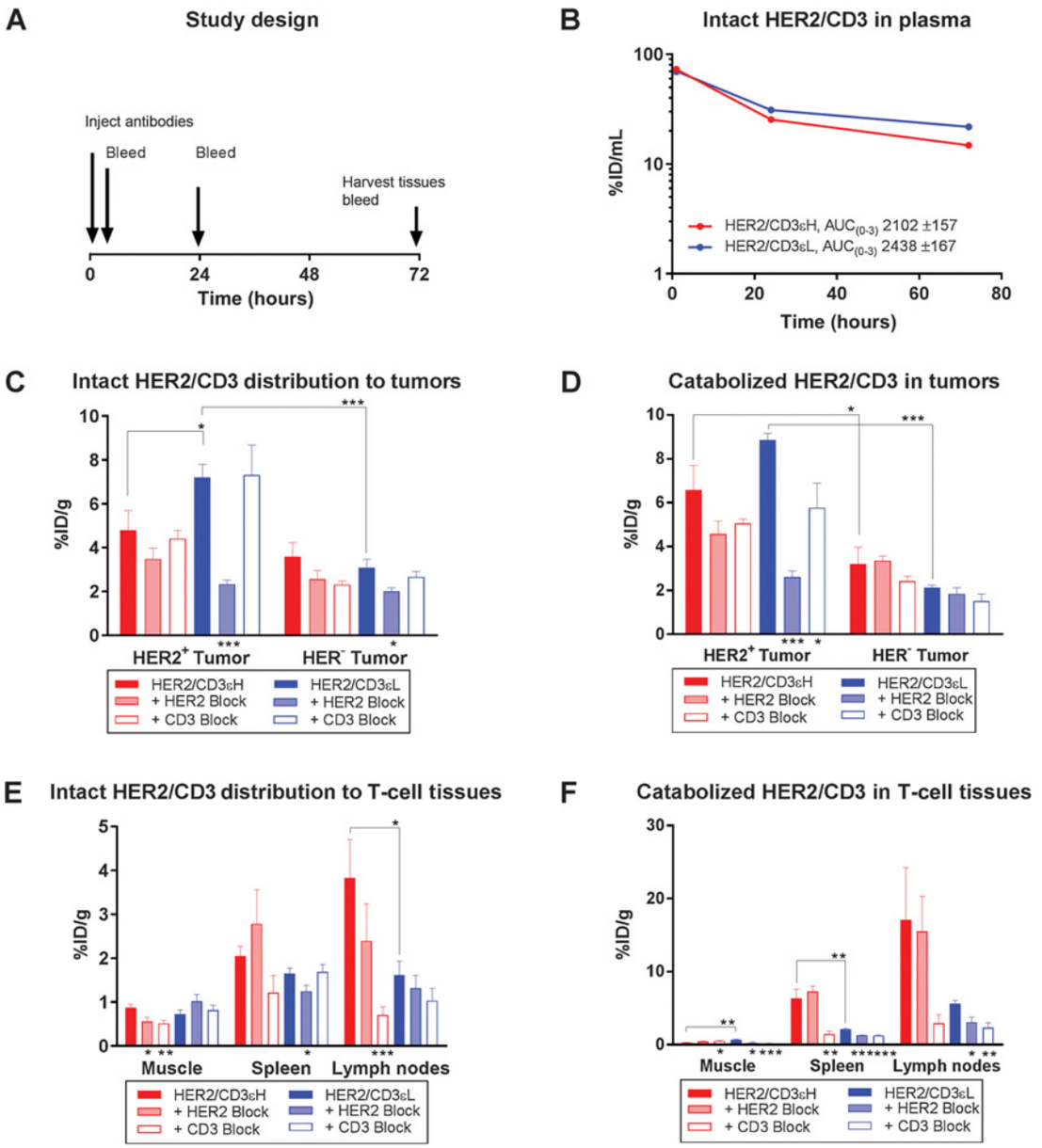

Figure 3.

Increased CD3 affinity negatively affects HER2/CD3 TDB tumor distribution and drives distribution to T-cell–containing tissues. **A,** Study design. The huCD3ε-TG mice bearing CT26 and huHER2-CT26 tumors on opposite flanks were injected with a single IV bolus of ^{125}I- and ^{111}In-labeled anti-HER2/CD3 TDBs (0.5 mg/kg) with low (CD3εL) or high (CD3εH) affinity to human CD3. Sparse blood samples were collected at 1, 24, and 72 hours. At 72 hours, mice were sacrificed for tissue distribution. Values are reported as a percentage of injected radioactive dose normalized to gram of dry blotted tissue (%ID/g) to convey changes in enrichment. In the groups denoted as "Block," the radiolabeled 0.5 mg/kg anti-HER2/CD3 TDB was coadministered with 50 mg/kg nonradiolabeled bivalent anti-CD3 antibody. **B,** Pharmacokinetics. Plasma levels of ^{125}I-radiolabeled antibody are represented as %ID/mL. AUC and AUC ± SEM values were calculated using GraphPad Prism, and significance was determined using a Student *t* test comparing the two exposures. **C–F,** Tissue distribution. Tissue concentrations of intact anti-HER2/CD3 antibodies expressed as ^{125}I (%ID/g) for (**C**) tumors and (**E**) T-cell–containing tissues. Catabolized antibody values in tumor were determined by subtracting the ^{125}I (%ID/g) from the ^{111}In (%ID/g) and plotted as catabolism (%ID/g) in (**D**) tumors and (**F**) T-cell–containing tissues. All graphs show mean ± SEM error bars of each group with $n = 5$. *P* values were obtained by the Student *t* test. HER2/CD3 TDB comparisons with corresponding blocks against HER2 or CD3 were indicated as significant with asterisks over the bars within each tissue. In addition, HER2/CD3εL and HER2/CD3εH were compared within and across HER2$^{+/-}$ tumors. Corresponding significance was indicated via brackets over the bars to clearly identify each significant comparison. All significant *P* values were reported as *, $P < 0.05$; **, $P \leq 0.01$; ***, and $P \leq 0.001$.

antibody (3.5 %ID/g intact and 4.6 %ID/g catabolized). Thus, the increased CD3 affinity of HER2/CD3εH significantly reduced the impact of the HER2 arm on tumor distribution. The lack of competition when blocking HER2 or CD3 in both tumors indicates that neither arm significantly drives distribution of HER2/CD3εH to tumors, suggesting that much of the uptake is

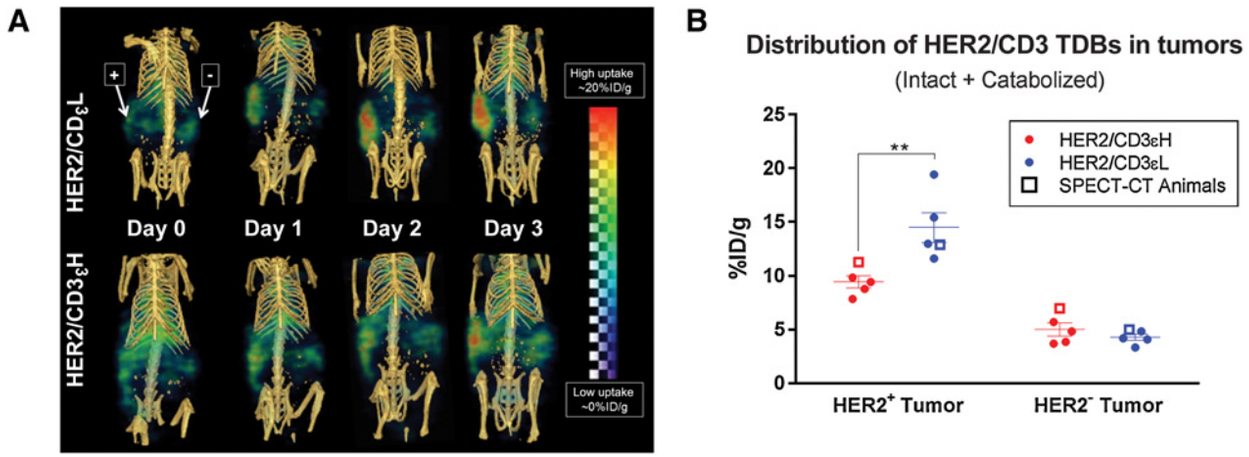

Figure 4.

Noninvasive SPECT-CT imaging of HER2/CD3 TBDs allows visualization of kinetics of tumor distribution. The huCD3ε-TG mice bearing CT26 and huHER2-CT26 tumors on opposite flanks were injected with ^{111}In-labeled anti-HER2/CD3 TDBs with low (CD3εL) and high (CD3εH) affinity to human CD3 at 5 mg/kg, representing distribution of both intact and catabolized TDBs. Mice were injected with a single IV bolus of approximately 400 uCi of ^{111}In-labeled TDB at 5 mg/kg and imaged at multiple time points using SPECT-CT. **A,** SPECT-CT images. All images were acquired consistently and visualized at the same exposure to depict changes in relative accumulation. **B,** Tissue distribution including SPECT-CT animals. Additional mice were injected with a single IV bolus of approximately 5 uCi of ^{111}In-labeled TDB at 5 mg/kg and subjected to tissue distribution analysis alongside the SPECT-CT mice 3 days after injection. The graphs show means ± SEM error bars of each group with $n = 5$, and p-values were obtained by Student's t-test versus control for each parameter tested. HER2/CD3εL and HER2/CD3εH were compared with each other by a Student *t* test, with brackets over the bars indicating the comparison and resulting *P* value. The HER2/CD3εL and HER2/CD3εH were compared across HER2-positive and -negative tumors with corresponding *P* values below the *x* axis. Square symbols represent SPECT-CT distribution data. All significant *P* values were reported as *, $P < 0.05$; **, $P \leq 0.01$; ***, $P \leq 0.001$.

nonspecific or non–receptor-mediated (Fig 3C and D). However, blocking the HER2 arm significantly reduced distribution and catabolism of HER2/CD3εL to HER2 tumors (Fig. 3C and D; $P < 0.001$) indicating HER2-dependent tumor distribution. HER2/CD3εH demonstrated poor HER2-dependent tumor distribution as indicated by similar distribution to both HER2-expressing and nonexpressing tumors (Fig. 3C). Similar intact (^{125}I) HER2/CD3εH signals were detected in HER2-positive (4.8 %ID/g) and -negative (3.6 %ID/g) tumors (Fig. 3C). Thus, increasing CD3 affinity significantly limits the impact of the HER2 arm on tumor distribution.

High CD3 affinity drives anti-HER2/CD3 TDB distribution to secondary lymphatic organs

In addition to measuring tumor distribution of TDBs, we also determined how CD3 affinity affects distribution to T-cell–containing tissues such as the spleen and lymph nodes in the presence of the tumor-targeting arm. In contrast to the dramatic changes observed in tumor accumulation, replacing the non–target-binding gD arm with the anti-HER2 arm did not alter the pattern of distribution. The HER2/CD3εH TDB demonstrated significantly higher CD3-dependent distribution to the lymph nodes compared with HER2/CD3εL (Fig. 3E; $P < 0.05$). HER2/CD3εH demonstrated intact distribution values of 2.1 %ID/g in spleen and 3.8 %ID/g in lymph nodes, whereas HER2/CD3εL had intact distribution values of 1.7 %ID/g in spleen and 1.6 %ID/g in lymph nodes (Fig. 3C). Interestingly, although HER2/CD3εH and HER2/CD3εL had similar intact distribution to the spleen, HER2/CD3εH had significantly higher catabolism (Fig. 3E and F; $P < 0.01$). These data together clearly show that increasing CD3 affinity dramatically increases distribution to secondary lymphatic tissues and negatively affects tumor distribution.

SPECT-CT imaging demonstrates that high CD3 affinity negatively affects HER2 tumor distribution kinetics

To observe longitudinal tumor uptake, we employed a noninvasive SPECT-CT imaging technique as an adjunct to the invasive biodistribution study (15, 16). The double-tumor–bearing huCD3ε-TG mice received a single intravenous injection of ^{111}In-labeled HER2/CD3 TDB (5 mg/kg), which is 10-fold higher in protein dose than in the invasive biodistribution arms. SPECT-CT allows whole-body imaging of antibody distribution and was performed at approximately 2, 24, 48, and 72 hours. Consistent with the nonimaging (invasive) distribution arms, HER2-dependent tumor distribution was observed with both HER2/CD3 TDBs, but was more striking for HER2/CD3εL (Fig. 4A). Within 48 hours, a clear increase in HER2$^+$ tumor accumulation was observed, particularly for HER2/CD3εL, and increased for the duration of the study. Accumulation of ^{111}In in tumors occurred sooner for HER2/CD3εL than for HER2/CD3εH (Fig. 4A). A modest HER2-independent accumulation was also observed in the HER2-negative tumor for both antibodies, possibly due to tumor-infiltrating T cells or alternatively due to nonspecific uptake. After noninvasive SPECT-CT image acquisitions, harvested tumor distribution was analyzed at 3 days as in the nonimaging studies. SPECT-CT animals were subjected to biodistribution analysis alongside 4 additional animals receiving only 5 μCi of radiolabeled TDB, but at a matched dose of 5 mg/kg. HER2/CD3εL showed significantly higher ($P < 0.01$) distribution of ^{111}In-labeled TDB in HER2$^+$ tumors compared with HER2/CD3εH (14.5 vs. 9.5 %ID/g, respectively, Fig. 4B). Both HER2/CD3εL and HER2/CD3εH exhibited significantly higher distribution in the HER2$^+$ tumors (14.5 and 9.5 %ID/g) compared with the HER2$^-$ tumors (4.3 and 5 %ID/g respectively in HER2$^-$ tumors, Fig. 4B). Taken together, these data indicate

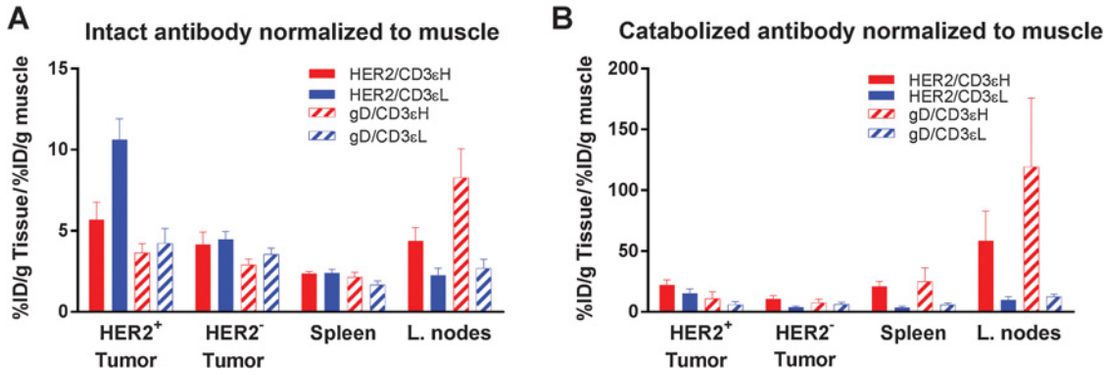

Figure 5.

Tissue and tumor distribution of HER2/CD3 TDBs represents a balance between CD3 and HER2 affinities. Data from gD/CD3 and HER2/CD3 distribution studies (Figs. 2 and 3) were normalized to muscle for direct comparison by dividing the %ID/g of each tissue by the %ID/g of the muscle measured for each individual animal. **A,** Intact antibody distribution. Tissue concentrations of intact (^{125}I) anti-HER2/CD3 antibodies expressed as %ID/g for tumor and T-cell–containing tissues. **B,** Catabolized antibody accumulation. Catabolized antibody values in tumor were determined by subtracting the ^{125}I %ID/g from the ^{111}In %ID/g, and plotted as the catabolism observed as %ID/g in tumors and T-cell–containing tissues.

that high CD3 affinity reduces HER2-dependent tumor distribution of anti-HER2/CD3 TDBs.

Tumor distribution of TDBs is dependent on balancing low CD3 affinity with the HER2 affinity

In order to compare data across two distinct biodistribution studies (Figs. 2 and 3), we normalized tumor distribution and catabolism to the corresponding data in muscle. Muscle tissue distribution is low and can be used to normalize tumor data against interanimal and interstudy variability in dosing and/or exposure. When comparing across studies, HER2/CD3 TDBs had increased distribution to HER2$^+$ tumors compared with the gD/CD3 TDBs. However, HER2/CD3$_\varepsilon$L had the most favorable tumor distribution among all variants (Fig. 5A).

Splenic distribution was relatively equal for both gD/CD3 and HER2/CD3 TDBs, but catabolism was the highest for HER2/CD3$_\varepsilon$H (Fig. 5B). Inclusion of the HER2 arm did not reduce splenic distribution, indicating that targeting HER2 does not interfere with spleen uptake (Fig. 5A). However, targeting HER2 (vs. gD) dramatically affected lymph node distribution. HER2/CD3$_\varepsilon$H had the highest distribution and catabolism in lymph nodes (Fig 5A and B). However, HER2/CD3 TDBs showed reduced lymphatic distribution compared with the gD/CD3 TDBs, suggesting some competition between the HER2$^+$ tumor and lymph nodes (Fig. 5A). Despite this competition, higher CD3 affinity still drove a higher proportion of the HER2/CD3 TDB to the lymph nodes (Fig. 5A).

Discussion

The work herein has demonstrated that, in the absence of tumor target arm binding, CD3 affinity is unimportant for tumor uptake but does affect systemic exposure and spleen/lymph node uptake (Fig. 2). Furthermore, in the presence of HER2-mediated tumor targeting, high CD3 affinity negatively affects HER2$^+$ tumor distribution while still driving uptake to secondary lymphatic tissues (Figs. 3–5). Overall, uptake in tumors reflects a fine balance between affinity for CD3 on T cells and HER2 on tumor cells, both of which are required for efficacy to some extent.

To our knowledge, no distribution studies have been published using preclinical models wherein the T-cell arm of the bispecific is actively bound to T cells. Nude mice are commonly employed to investigate the biodistribution and tumor uptake of TDBs (17, 18), but they lack endogenous T cells. CD3 antibodies do not crossreact between human and mouse CD3 orthologues, which substantially complicates preclinical *in vivo* pharmacology of CD3-bispecific antibodies. Typical *in vivo* efficacy models consist of a human xenograft tumor grafted into immunecompromised mice. Human T cells are used as effectors either by cograftment with the tumor cells or by spatially and temporally separated injection into the intraperitoneal cavity. Although these "humanized" mice provide robust models for proof-of-concept antitumor activity and dose-response studies, the value for other *in vivo* pharmacology readouts such as target-dependent clearance and tissue distribution is limited. As a consequence, very little is known about the effect of affinities on *in vivo* properties of CD3-bispecific antibodies.

To overcome this challenge, we exploited a unique preclinical mouse model which expresses the human CD3 epsilon in T cells (huCD3ε-TG mice) to evaluate systemic *in vivo* properties of human CD3-specific TDB (14). T cells in these mice express both mouse and human CD3 at approximately 50% levels respective to Balb/c mouse or human T cells (10). The human CD3ε subunit can both structurally and functionally substitute for murine CD3ε in the transgenic mouse. To appropriately investigate the role of target competition, we selected a model that also recapitulates both targets of the TDB (i.e., HER2 and CD3). huCD3ε-TG T cells can kill human HER2-expressing target cells *in vitro* either through stimulation with huCD3 or murine CD3-reactive TDBs (10). Syngeneic CT26 tumors engineered to express human HER2 (CT26-HER2) are partially sensitive to HER2 TDB treatment in huCD3ε-TG mice in efficacy studies, although PD-1/PDL-1 signaling substantially limits the activity (10).

Our results with the gD/CD3 TDB, which binds to T cells while the target arm is nonbinding, demonstrated that CD3 affinity had a dramatic impact on systemic TDB distribution and exposure (Fig. 2). Previous reports suggested that low CD3 affinity is also desirable to avoid trapping of the TDB by circulating T cells and their activation (19). Furthermore, the observed increase in target-mediated clearance (i.e., reduced exposure) by high T-cell affinity is consistent with results observed with the CLL-1–targeting TDB

(12). In our studies, higher CD3 affinity ($\leq$1 nmol/L) molecules accumulated in T-cell–rich tissues such as the spleen and lymph nodes, whereas 50 nmol/L CD3 affinity was not sufficient to drive distribution to these secondary lymphatic organs (Fig. 2). In the absence of target-driven distribution, isolated T-cell affinity alone was not sufficient to affect the tumor localization of gD/CD3 TDBs (Fig. 2). However, when a HER2-binding target arm was incorporated into the TDB, high CD3 affinity impaired HER2-dependent tumor distribution of anti-HER2/CD3 TDBs (Fig. 3). The negative impact of increased CD3 affinity on HER2-dependent tumor uptake was also observed in a longitudinal noninvasive SPECT imaging study (Fig. 4). Higher CD3 affinity increased distribution to T-cell–containing tissues while decreasing tumor distribution, indicating that the relative affinity between the two arms of the TDB imparted competition affecting both distribution and exposure. These distribution differences warrant attention for their potential impacts on therapeutic indices of clinical candidates and the overall design process for TDBs.

In many cases, therapeutic antibody design strategy is driven by striving for the highest attainable antigen-binding affinity (20, 21). However, in the case of TDB design, more factors have to be considered because there are two distinct targets, each with its own tissue expression profile, on/off rates of antigen binding, and turnover rate. We observed higher amounts of catabolism with higher CD3 affinity variants in secondary lymphatic tissues (Figs. 2 and 3), suggesting that lower CD3 affinity is preferable to avoid high distribution to secondary lymphatic tissues and CD3-mediated plasma clearance of TDB. However, a portion of TDB bound to T cells in lymphoid organs might still be able to reenter circulation and traffic to other tissues including tumor. Tumor antigen turnover rates and/or antigen shedding can also affect TDB distribution. Cell surface HER2 in human breast cancer has a slow turnover rate and is resistant to downregulation. Consistently, trastuzumab binding does not induce HER2 downregulation but rather passively recycles after HER2 endocytosis (22, 23). For a TDB with a rapidly internalizing tumor target, lower tumor target affinity might be desirable to lower the risk of rapid depletion, whereas slowly internalizing tumor targets might benefit from higher affinity. A high CD3 affinity arm could prompt increased cytolytic synapse formation, thereby decreasing the tumor receptor–mediated internalization rate (24). However, the work herein underscores the importance of balancing this with the tumor-targeting arm to achieve a desirable affinity-driven distribution. Future work that utilizes modeling of TDB affinities and turnover rates will enable a better characterization of what combinations are ideal on a case-by-case basis.

Although bivalent anti-CD3 antibodies can activate T cells and elicit massive cytokine release, monovalent anti–CD3-bispecific antibodies are much weaker at inducing T-cell activation in the absence of target cell recognition and are thus expected to be more tolerable (25, 26). However, safety of TDBs must still be assessed, and addressing the potential impact of CD3 affinity on safety has unfortunately been a challenge in preclinical species. TDBs with CD3 affinity in the nanomolar range had increased distribution to secondary lymphatic tissue which may lead to off-target toxicity (Figs. 2–5). Previous studies with TDBs that have CD3 affinity in a similar range observed grade Ill–IV toxicity at selected doses within an hour of infusing a folate receptor/CD3-bispecific antibody in ovarian cancer patients, prompted by coating of peripheral T cells with the bispecific antibody and subsequent T-cell activation and cytokine release (27). Furthermore, increasing CD3 or another TCR component affinity could have similar negative safety implications. For example, in clinical trials involving T-cell–activating therapies, patients need to be monitored for hemophagocytic lymphohistiocytosis and any other symptoms of cytokine-related illnesses (28). Severe reactions have been reported with CD3-directed TDBs in the clinic (28), including death in EpCAM/CD3 TDB phase I clinical trials (29), all of which resulted from overactivation of T cells. Although our model was beneficial in determining a more clinically relevant tissue distribution by actively binding the mouse's T cells, it is still not a valid safety model and these efforts will be reported elsewhere. Nevertheless, our data indicate a clear platform from which these issues could arise, and support utilizing TDBs with lower CD3 affinities which retain HER2-mediated tumor targeting while avoiding issues that could potentially arise from distribution to T-cell–containing tissues.

In addition to understanding how target arm affinities affect distribution, the effects on formation of functional cytolytic synapses with the target cell are also crucial for TDB design and selection. Our dual-tracer approach included both nonresidualizing radiohalogen (^{125}I) and residualizing radiometal-chelate (^{111}In-DOTA) labels to simultaneously detect intact and total (including catabolized) protein uptake, respectively. This partially addresses the intended mechanism of action, as only cell surface or interstitial (i.e., nondegraded) TDB, reflected by the ^{125}I label, would still be capable of synapse formation. However, one major limitation of our experimental approach is that we are unable to conclusively differentiate among radiolabeled TDB that is T-cell–associated, HER2-associated, or bridged between both cell types, the latter of which is the active drug form. In other words, our radioanalytical method was unable to verify the extent, if at all, to which synapse formation has occurred. If TBD initially distributes to tumor, T-cell engagement must still occur. Conversely, binding of TDB to T cells could occur first, raising the important question of how much T-cell–associated TDB can still effectively distribute to tumor.

The design of TDBs and other bispecific antibodies is a complex endeavor that requires consideration of multiple parameters. We have shown that balancing the binding of both targeting arms of the TDB to their respective targets affects distribution to tumor and T-cell-rich tissues, each of which may ultimately influence efficacy and/or safety. Future studies exploring how these precisely relate to each other will provide a more informed design process for future TDB therapeutics.

Disclosure of Potential Conflicts of Interest

No potential conflicts of interest were disclosed.

Authors' Contributions

Conception and design: D. Mandikian, J. Li, K. Lin, S.B. Joseph, M.S. Dennis, S. Prabhu, T.T. Junttila, C.A. Boswell

Development of methodology: D. Mandikian, A.A. Lo, J. Li, K. Lin, T.T. Junttila, C.A. Boswell

Acquisition of data (provided animals, acquired and managed patients, provided facilities, etc.): D. Mandikian, N. Takahashi, A.A. Lo, J. Li, J. Eastham-Anderson, D. Slaga, J. Ho, R. Clark, K. Totpal, K. Lin, C.A. Boswell

Analysis and interpretation of data (e.g., statistical analysis, biostatistics, computational analysis): D. Mandikian, A.A. Lo, J. Li, J. Eastham-Anderson, K. Lin, S.B. Joseph, M.S. Dennis, S. Prabhu, T.T. Junttila, C.A. Boswell

Writing, review, and/or revision of the manuscript: D. Mandikian, A.A. Lo, J. Li, K. Totpal, K. Lin, S.B. Joseph, S. Prabhu, T.T. Junttila, C.A. Boswell

Administrative, technical, or material support (i.e., reporting or organizing data, constructing databases): D. Mandikian

Study supervision: D. Mandikian, S.B. Joseph, T.T. Junttila

Acknowledgments

The authors would like to thank Sid Sukumaran, Kapil Gadkar, Meric Ovacic, and Simon Williams for helpful discussions; Allison Bruce for assistance with illustrations; and Sheila Ulufatu, Michelle Schweiger, Jose Imperio, Kirsten Messick, Nicole Valle, Cynthia Young, Elizabeth Torres, Nina Ljumanovic, Bernadette Johnstone, Shannon Liu, Konnie Urban, Christopher Stevenson, Ka Man Li, and Shannon Stainton for technical support.

The costs of publication of this article were defrayed in part by the payment of page charges. This article must therefore be hereby marked *advertisement* in accordance with 18 U.S.C. Section 1734 solely to indicate this fact.

Received July 11, 2017; revised November 7, 2017; accepted December 19, 2017; published OnlineFirst January 16, 2018.

References

1. Siegel RL, Miller KD, Jemal A. Cancer statistics, 2016. CA Cancer J Clin 2016;66:7–30.
2. Jackisch C, Lammers P, Jacobs I. Evolving landscape of human epidermal growth factor receptor 2-positive breast cancer treatment and the future of biosimilars. Breast 2017;32:199–216.
3. Chung A, Cui X, Audeh W, Giuliano A. Current status of anti-human epidermal growth factor receptor 2 therapies: predicting and overcoming herceptin resistance. Clin Breast Cancer 2013;13:223–32.
4. Li J, Stagg NJ, Johnston J, Harris MJ, Menzies SA, DiCara D, et al. Membrane-proximal epitope facilitates efficient T cell synapse formation by Anti-FcRH5/CD3 and is a requirement for myeloma cell killing. Cancer Cell 2017;31:383–95.
5. Chames P, Baty D. Bispecific antibodies for cancer therapy: the light at the end of the tunnel? MAbs 2009;1:539–47.
6. Brischwein K, Schlereth B, Guller B, Steiger C, Wolf A, Lutterbuese R, et al. MT110: a novel bispecific single-chain antibody construct with high efficacy in eradicating established tumors. Mol Immunol 2006;43: 1129–43.
7. Dreier T, Baeuerle PA, Fichtner I, Grün M, Schlereth B, Lorenczewski G, et al. T cell costimulus-independent and very efficacious inhibition of tumor growth in mice bearing subcutaneous or leukemic human B cell lymphoma xenografts by a CD19-/CD3- bispecific single-chain antibody construct. J Immunol 2003;170:4397–402.
8. Sun LL, Ellerman D, Mathieu M, Hristopoulos M, Chen X, Li Y, et al. Anti-CD20/CD3 T cell-dependent bispecific antibody for the treatment of B cell malignancies. Sci Transl Med 2015;7:287ra70.
9. Topp MS, Gökbuget N, Stein AS, Zugmaier G, O'Brien S, Bargou RC, et al. Safety and activity of blinatumomab for adult patients with relapsed or refractory B-precursor acute lymphoblastic leukaemia: a multicentre, single-arm, phase 2 study. Lancet Oncol 2015;16:57–66.
10. Junttila TT, Li J, Johnston J, Hristopoulos M, Clark R, Ellerman D, et al. Antitumor efficacy of a bispecific antibody that targets HER2 and activates T cells. Cancer Res 2014;74:5561–71.
11. Atwell S, Ridgway JB, Wells JA, Carter P. Stable heterodimers from remodeling the domain interface of a homodimer using a phage display library. J Mol Biol 1997;270:26–35.
12. Leong SR, Sukumaran S, Hristopoulos M, Totpal K, Stainton S, Lu E, et al. An anti-CD3/anti-CLL-1 bispecific antibody for the treatment of acute myeloid leukemia. Blood 2017;129:609–618.
13. Shalaby MR, Shepard HM, Presta L, Rodrigues ML, Beverley PC, Feldmann M, et al. Development of humanized bispecific antibodies reactive with cytotoxic lymphocytes and tumor cells overexpressing the HER2 proto-oncogene. J Exp Med 1992;175:217–25.
14. de la Hera A, Müller U, Olsson C, Isaaz S, Tunnacliffe A. Structure of the T cell antigen receptor (TCR): two CD3 epsilon subunits in a functional TCR/CD3 complex. J Exp Med 1991;173:7–17.
15. Pastuskovas CV, Mundo EE, Williams SP, Nayak TK, Ho J, Ulufatu S, et al. Effects of anti-VEGF on pharmacokinetics, biodistribution, and tumor penetration of trastuzumab in a preclinical breast cancer model. Mol Cancer Ther 2012;11:752–62.
16. Boswell CA, Mundo EE, Firestein R, Zhang C, Mao W, Gill H, et al. An integrated approach to identify normal tissue expression of targets for antibody-drug conjugates: case study of TENB2. Br J Pharmacol 2013; 168:445–57.
17. Reusch U, Duell J, Ellwanger K, Herbrecht C, Knackmuss SH, Fucek I, et al. A tetravalent bispecific TandAb (CD19/CD3), AFM11, efficiently recruits T cells for the potent lysis of CD19(+) tumor cells. MAbs 2015;7:584–604.
18. Warnders FJ, Waaijer SJ, Pool M, Lub-de Hooge MN, Friedrich M, Terwisscha van Scheltinga AG, et al. Biodistribution and PET imaging of labeled bispecific T cell-engaging antibody targeting EpCAM. J Nucl Med 2016;57:812–7.
19. List T, Neri D. Biodistribution studies with tumor-targeting bispecific antibodies reveal selective accumulation at the tumor site. MAbs 2012; 4:775–83.
20. Carter PJ. Potent antibody therapeutics by design. Nat Rev Immunol 2006;6:343–57.
21. Lippow SM, Wittrup KD, Tidor B. Computational design of antibody-affinity improvement beyond in vivo maturation. Nat Biotechnol 2007; 25:1171–6.
22. Austin CD, De Mazière AM, Pisacane PI, van Dijk SM, Eigenbrot C, Sliwkowski MX, et al. Endocytosis and sorting of ErbB2 and the site of action of cancer therapeutics trastuzumab and geldanamycin. Mol Biol Cell 2004;15:5268–82.
23. Bertelsen V, Stang E. The mysterious ways of ErbB2/HER2 trafficking. Membranes (Basel) 2014;4:424–46.
24. Andersen PS, Geisler C, Buus S, Mariuzza RA, Karjalainen K. Role of the T cell receptor ligand affinity in T cell activation by bacterial superantigens. J Biol Chem 2001;276:33452–7.
25. Moore GL, Bautista C, Pong E, Nguyen DH, Jacinto J, Eivazi A, et al. A novel bispecific antibody format enables simultaneous bivalent and monovalent co-engagement of distinct target antigens. MAbs 2011;3:546–57.
26. Moore PA, Zhang W, Rainey GJ, Burke S, Li H, Huang L, et al. Application of dual affinity retargeting molecules to achieve optimal redirected T-cell killing of B-cell lymphoma. Blood 2011;117:4542–51.
27. Tibben JG, Boerman OC, Massuger LF, Schijf CP, Claessens RA, Corstens FH. Pharmacokinetics, biodistribution and biological effects of intravenously administered bispecific monoclonal antibody OC/TR F(ab')2 in ovarian carcinoma patients. Int J Cancer 1996;66:477–83.
28. Teachey DT, Rheingold SR, Maude SL, Zugmaier G, Barrett DM, Seif AE, et al. Cytokine release syndrome after blinatumomab treatment related to abnormal macrophage activation and ameliorated with cytokine-directed therapy. Blood 2013;121:5154–7.
29. Mau-Sorensen M, Dittrich C, Dienstmann R, Lassen U, Büchler W, Martinius H, et al. A phase I trial of intravenous catumaxomab: a bispecific monoclonal antibody targeting EpCAM and the T cell coreceptor CD3. Cancer Chemother Pharmacol 2015;75:1065–73.